# X-ray Absorption Spectroscopy for the Characterization of Photoinduced Linkage Isomers in Single Crystals: Experimental Setup and XANES Results**

Duclair Tchana Kamgne, Bridinette Thiodjio Sendja, Danilo Oliveira de Souza, Theo Woike, Giuliana Aquilanti, Dominik Schaniel

# X-ray Absorption Spectroscopy for the Characterization of Photoinduced Linkage Isomers in Single Crystals: Experimental Setup and XANES Results

Duclair Tchana Kamgne[a], Prof. Dr. Bridinette Thiodjio Sendja[b], Dr. Danilo Oliveira de Souza[c], Prof. Dr. Theo Woike[d] Dr. Giuliana Aquilanti[c], Prof. Dr. Dominik Schaniel[d*],

[a]*University of Yaounde I, Faculty of Science, Department of Physics, Yaounde, Cameroon*
[b]*University of Yaounde I, National Advanced School of Engineering, Department of Mathematic and Physical Science, Yaounde, Cameroon*
[c]*Elettra –Sincrotrone Trieste, s.s. 14 - km 163,5 in AREA Science Park, 34149 Basovizza, Trieste, Italy*
[d]*Université de Lorraine, CNRS, CRM2, 54000 Nancy, France*
*Corresponding author. dominik.schaniel@univ-lorraine.fr

## Abstract

Photoinduced linkage isomers (PLI) of the nitrosyl ligand in single crystals of $Na_2[Fe(CN)_5NO]\cdot 2H_2O$ (SNP, sodium nitroprusside) have been studied by X-ray absorption spectroscopy (XAS) at low temperatures, using a cryostat allowing in-situ polarized LASER irradiation and XAS measurements. In the XANES (X-ray Absorption Near Edge Structure) region a significant modification of the pre-edge peak intensities is observed after irradiation of the ground state (GS) nitrosyl NO-κ*N* isomer with light in the blue and infrared spectral range, used for the generation of the isonitrosyl NO-κ*O* isomer (MS1) and the side-on bound $\kappa^2$*N,O* isomer (MS2), respectively. These observations are interpreted with respect to the changes in the nature of the frontier (unoccupied) molecular orbitals of the different linkage isomer configurations, expected from earlier calculations.

## Introduction

The manipulation of molecular compounds by light is of interest in various domains, ranging from medicine and biology to optics, e.g. the photoinduced ligand-release is of interest in photodynamic therapy [1] while the photochromic and photorefractive properties might be exploited in optoelectronic and photonic applications [2]. One particular class of photosensitive materials are transition-metal nitrosyl complexes which can be used for both medical and optical applications, by either photoinduced NO release or the generation of photoinduced linkage isomers (PLI) of the NO ligand [3]. Studying the bonding and activation of NO is essential for a comprehensive understanding of these two competing processes. Various structural types of PLI can be generated in mono- and dinitrosyl complexes, depending on the electronic configuration [4]. In the Enemark-Feltham notation [5], $\{MNO\}^n$ for mono-nitrosyl complexes (M = metal), *n* is the number of metal-d electrons if the ligand is assumed as $NO^+$. For systems with $n \leq 6$, the ground state (GS) configuration is in general a linear MNO. $Na_2[Fe(CN)_5NO]\cdot 2H_2O$ (SNP, sodium nitroprusside) is the prototypical example for a $\{MNO\}^6$ system. As illustrated in Scheme 1, three linkage isomers of NO can be found in such an octahedral mono-nitrosyl compound, the ground state (GS) configuration corresponding to the nitrogen bound linear linkage of NO (NO-κ*N*), and two so-called metastable states (MS). MS1 corresponds to the oxygen bound linear linkage of NO (κO, isonitrosyl) while MS2 to a side-

on bound configuration of the NO ($\kappa^2 N,O$) with respect to the central metal atom [6]. As discussed recently [4], the metal-nitrosyl bond in SNP is established through the interplay of three interactions: two Fe-to-NO π-backbonds from the low-spin-$d^6$ metal's occupied d(xz) and d(yz) atomic orbitals (AO) (z is along the Fe–NO axis) to the empty N–O-π* molecular orbital (MO), and the NO-to-Fe donor bond from the N-atom's lone pair to the iron's empty d($z^2$) AO. For GS and MS1 this results in a linear M–N–O and M–O–N configuration, essentially due to the fact that the N(O)-atom's lone pair can interact with the empty d($z^2$) of the iron. The side-on MS2 configuration is stabilized through the interaction of the N–O-π-bond in the FeNO plane with the empty d($z^2$) of the iron.

Conversion between the three linkage isomers is possible by light, forward and backward reactions being induced by different wavelengths. In general, irradiation in the blue-green spectral range transforms GS towards MS1 and MS2, while irradiation with red and infrared light leads to the backward reaction from MS1,2 towards GS [7]. Infrared light can be used to transform MS1 towards MS2. MS1 and MS2 are stable at low temperatures since they are separated from each other and the GS by activation barriers of the order of 0.3-1 eV, hence the name metastable state. Depending on the composition, the wavelength ranges for interconversion as well as the heights of the activation barriers vary [8].

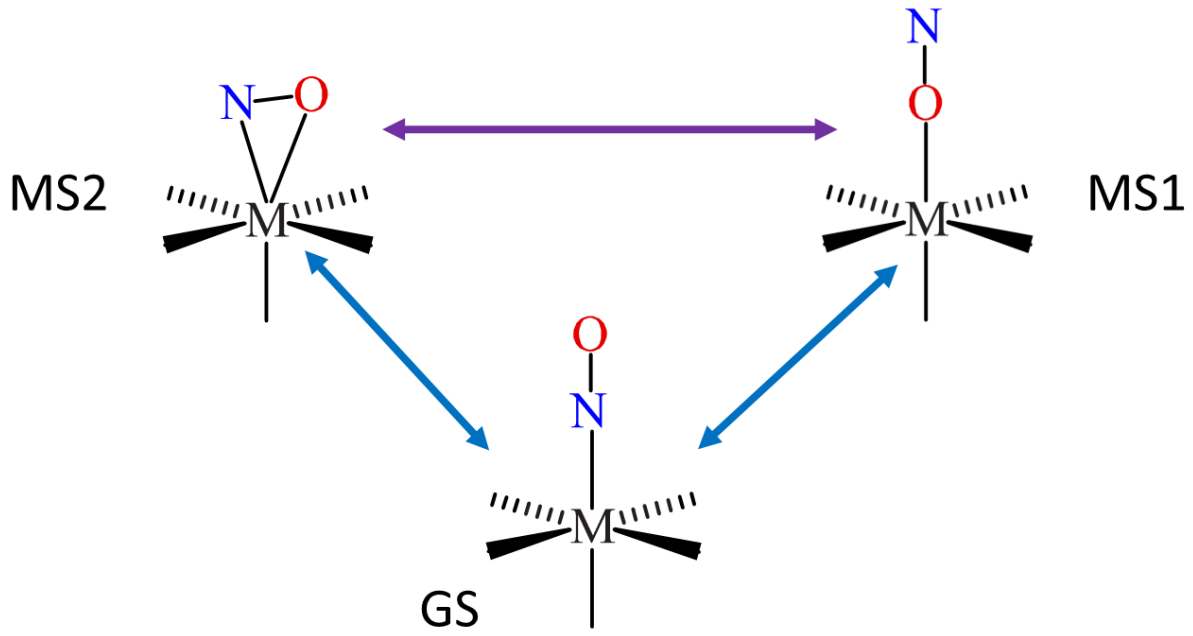


Scheme 1: Linkage isomer configuration for $\{MNO\}^6$ type mono-nitrosyl complexes such as $[Fe(CN)_5(NO)]^{2-}$ in SNP [4]. GS denotes the energetic ground state corresponding to the N bound linear M–N–O linkage (NO-κ*N*). MS1 is the so-called isonitrosyl configuration with an O-bound linear M–O–N linkage (NO-κ*O*), and MS2 is the side-on configuration of the NO ligand ($\kappa^2 N,O$).

For the design and improvement of the application-related properties, a comprehensive understanding of the underlying photophysical and photochemical mechanisms is essential. Therefore, a large number of experimental methods have been applied for the (in-situ) study of these photoinduced processes spanning the time scales from femtoseconds to hours, especially

for the prototype compound SNP. Of major interest is the detailed knowledge about the excitation and relaxation mechanisms and pathways, which in turn requires the investigation of the electronic and structural properties of the photoinduced species, at various time points. Static UV/Vis and Infrared spectroscopy [9,10], calorimetry [11], Mössbauer spectroscopy [12], X-ray and neutron diffraction [13] have been used (at low temperatures) and in combination with theoretical calculations [14] provided a rather complete description of the PLI. Time-resolved spectroscopy (UV/Vis, Infrared, photoelectron) [15] has been used to elucidate the photoisomerization process and determine the characteristic time scales for the rotation of the NO ligand. Up to now no direct time resolved observation of this photoinduced structural reorganization by diffraction or related methods has been reported, except for the relaxation of the PLI back to GS by X-ray diffraction (XRD) on the millisecond time scale [16]. X-ray absorption spectroscopy (XAS) offers the possibility to study both, the electronic and structural properties [17] and can thus be used to investigate also the corresponding photoinduced changes. For example, photoinduced valence tautomerism [18], local structural changes of trapped photoexcited states in magnetic cobalt compounds [19] or photoinduced magnetic phase transitions [20] have been studied by XAS at low temperature under illumination. Polarized XAS has been used to study the photoinduced Fe–CO bond breaking including a study of the pre-edge region yielding insight into the electronic structure of the frontier molecular orbitals [21]. Furthermore, ultrafast XAS has been developed and applied for the study of photoexcited systems, see e.g. [22] and these methods are now available at various synchrotron sources allowing for the study of short-lived photoinduced species. Nevertheless, the study of the PLI phenomenon in transition-metal nitrosyl compounds has been attempted only once using XAS [23], however no changes in the spectra could be observed in this early study. Besides, the GS of SNP has been characterized using Fe L-edge XAS [24] and Fe K-edge XAS [25].

In order to open the way for the use of XAS for the characterization of PLI in transition-metal nitrosyl complexes, we performed low-temperature polarized XAS on single crystals of the prototype material SNP under light-irradiation. We successfully generated the two types of metastable linkage isomers, MS1 and MS2, by applying an appropriate light irradiation sequence. The observed changes in the pre-edge peak intensities are discussed with respect to the changes in the frontier molecular orbitals as predicted from earlier theoretical calculations. Our results provide the first XAS fingerprints of the PLI species and as such will be useful for preparing future measurements in time-resolved mode as well as for the study of photoswitchable non-crystalline hybrid materials (molecule@matrix) by XAS.

## Results and discussion

Several crystals of different thickness (between 80 and 130 μm) were measured in GS and after light irradiation (with different exposure times) in order to determine the light induced changes occurring in the XAS spectra upon generation of MS1 (blue light) and subsequent transfer to MS2 (infrared light). The light polarization was chosen along the crystallographic *c*-axis in order to maximize population of the metastable states [7]. In view of the orientation of the quasi fourfold N–C–Fe–N–O axis, which is in the *ab*-plane (see experimental details

and Figure 1 in [25]), the polarization of the X-ray beam was chosen perpendicular to the *c*-axis, thereby guaranteeing the presence of dipole-allowed transitions in the pre-edge area (*vide infra*). The pre-edge region of all spectra is characterized by a well-resolved peak A at about 7114 eV and two shoulder peaks B and C at about 7119 and 7122 eV, respectively, in agreement with previous results collected at room temperature on SNP single crystals when choosing X-ray polarization along *a* or *b* crystallographic axes [25]. Figure 1 shows as an example the results on the 80 μm crystal in the range 7100 – 7250 eV. The edge is found at 7131.8 eV, and its position is not changed upon irradiation. This clearly indicates that the oxidation state of iron does not change upon photoisomerization, as is expected from earlier results, e.g. Mössbauer spectroscopy [12]. On the other hand, intensity changes are observed at several positions, especially also in the pre-edge peak A at about 7114 eV. Looking into more detail in the evolution of this pre-edge peak as a function of irradiation wavelength and duration we observe the following behavior. Upon irradiation with 476 nm we observe an increase in the intensity of the pre-edge peak, while the position of the peak does not change within the resolution of our experiment. Compared to GS, the integrated area under the peak is increased by about 17% after 15 hours of irradiation, corresponding to $Q$ = 1080 J/cm$^2$, as illustrated in Figure 2 for a crystal with thickness 130 μm The subsequent irradiation with 1064 nm leads to a decrease of the intensity of this peak. After 90 minutes of irradiation, corresponding to $Q$ = 270 J/cm$^2$, the intensity has decreased to about 1.07 times the intensity of GS. Both, the increase upon blue light irradiation and the decrease upon infrared light irradiation follow a monoexponential behavior with time constants $Q_{blue}$ = 205(31) J/cm$^2$ and $Q_{infrared}$ = 197 (190) J/cm$^2$. The same behavior is observed for other crystals with thicknesses 80, 90, 110 μm, for which the X-ray polarization was always chosen perpendicular to the *c*-axis of the crystal.

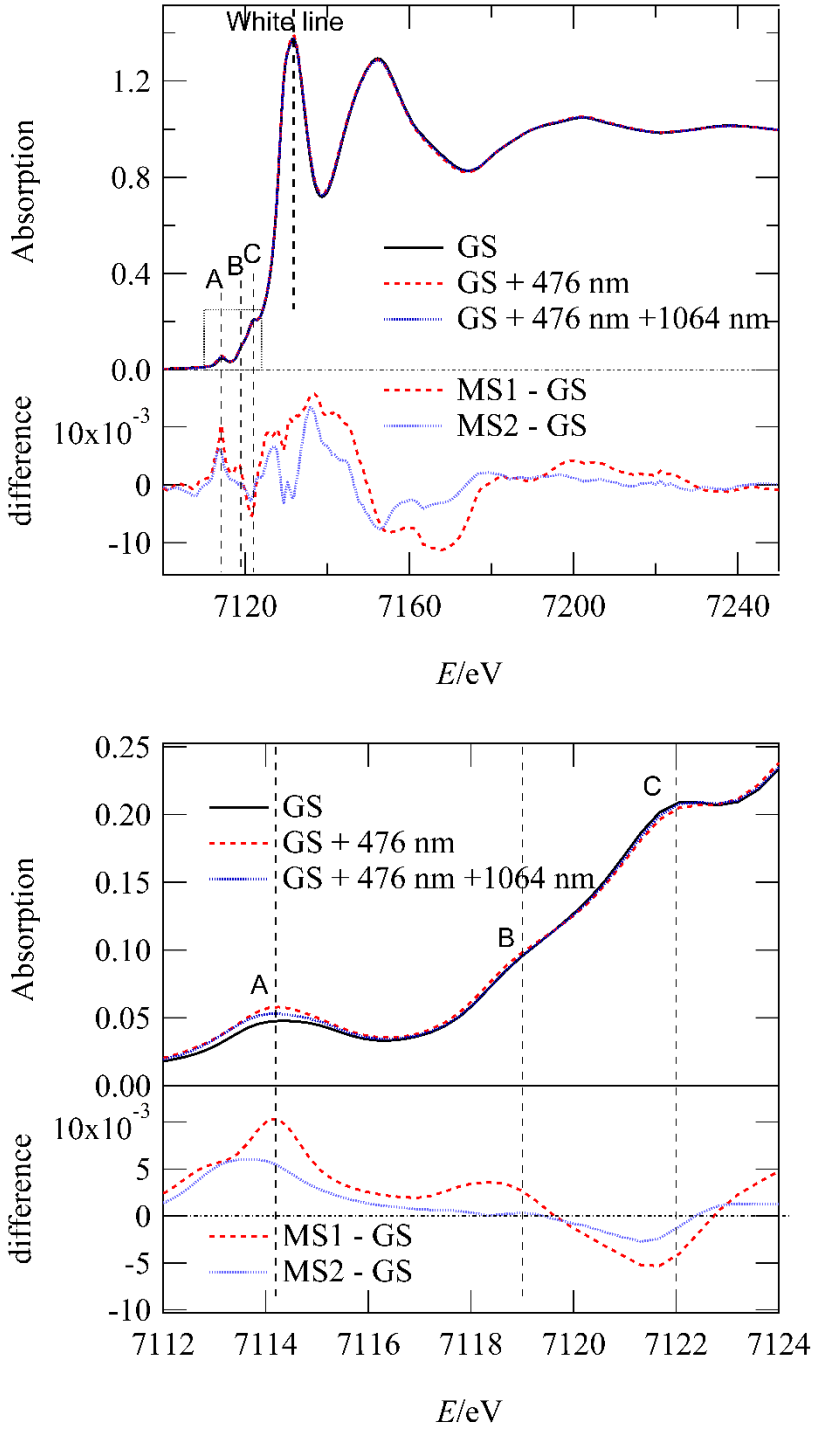


Figure 1: XAS spectra for an 80 µm thick crystal (a-cut, polarization of X-ray beam perpendicular to the *c*-axis of the crystal, i.e. with a component parallel to the Fe–N–O direction): GS (black line), after irradiation with 476 nm light (red dashed line) and subsequent irradiation with 1064 nm (blue dotted line). A, B, C denote pre-edge features at 7114, 7119, and 7122 eV, respectively. (Top) Full range 7100 – 7250 eV and corresponding difference spectra. (Bottom) Zoom in the range 7110 – 7124 eV.

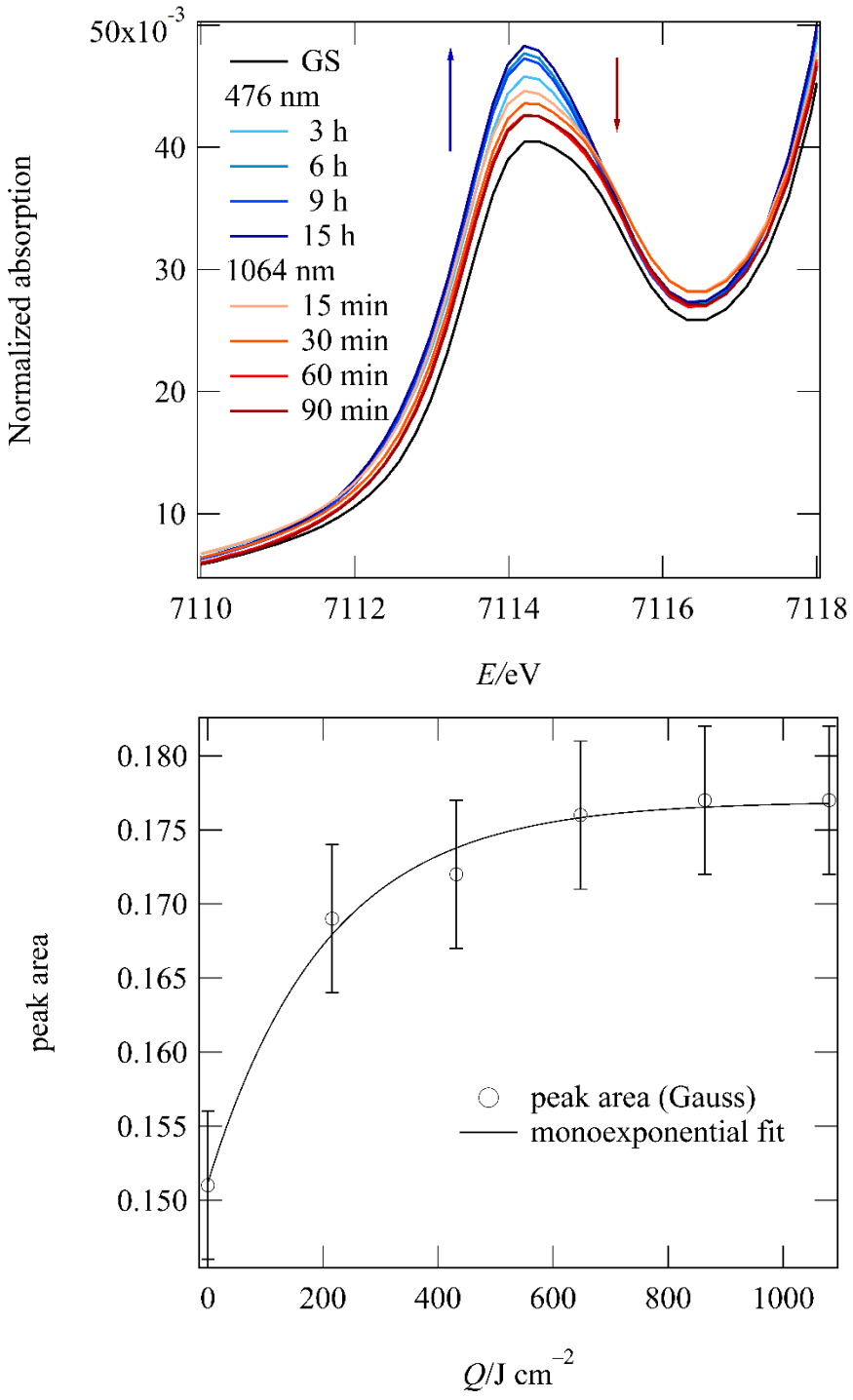


Figure 2: (top) XAS spectra in the range 7110 – 7118 eV for a 130 µm thick crystal (b-cut, polarization of X-ray beam perpendicular to *c*-axis) in the GS (black line), after irradiation with 476 nm light and subsequent irradiation with 1064 nm. (bottom) Integrated area of pre-edge peak as a function of irradiation exposure *Q* and corresponding monoexponential fit for the increase upon irradiation with 476 nm.

The fact that we do observe an increase of the pre-edge peak intensity (but no measureable energetic shift) indicates that the transition probability at the origin of this peak changes after light irradiation, upon population of the MS1 state. For a qualitative analysis of this observation we recall that the pre-edge peaks in 3d transition-metal compounds can be of dipolar or quadrupolar character [26]. In SNP the electronic configuration of the iron metal center is low-spin $d^6$ and the point symmetry of the molecule is (nearly) $C_{4v}$. The z-axis is chosen along the quasi-fourfold rotation axis N–C–Fe–N–O. From ligand field theory we expect thus a splitting of the $e_g$ into two orbitals ($d(z^2)$; $d(x^2-y^2)$) and of the $t_{2g}$ into three orbitals (d(xz,yz); d(xy)) with an energetically degenerate d(xz,yz). The significant back-bonding with the NO ligand leads to the lowering of the antibonding π*(NO) orbital, which constitutes the LUMO (with significant d-character). UV/Vis absorption spectroscopy combined with DFT calculations established this energetic level scheme [9, 27], the LUMO being the π*(NO) with E symmetry, the LUMO+1 the mainly $d_{z2}$ with A1 symmetry and the LUMO+2 the mainly $d(x^2-y^2)$ with B1 symmetry. The LUMO and LUMO+1, LUMO+2 are separated by ca. 0.7 – 1.5 eV (see Figure 3)[9]. According to previous XAS studies on the GS of SNP, the first pre-edge peak at about 7114 eV might correspond to a transition to either of these final states by promoting an electron from 1s to the π*(NO), the $d(z^2)$, or the $d(x^2-y^2)$. Since the π*(NO) orbital has significant p-orbital character (from O and N) dipole allowed transitions can be expected due to a transition 1s → π*(NO) while 1s → $d(z^2)$ and 1s → $d(x^2-y^2)$ are expected to be of quadrupolar nature. However, as calculations have shown [9], also the mainly $d(z^2)$ has a significant amount of ligand p-contribution (from Np(z) in GS and from Op(z) in MS1), so that the 1s → $d(z^2)$ should be potentially considered as a dipole allowed transition. In $C_{4v}$ symmetry the dipole moment operator has the form (E,E,A1). The final state generated by a 1s → π*(NO) transition has A1 x E = E symmetry (1s being total symmetric A1) and hence the product A1 x (E,E,A1) x E yields (A1, A1, E) for (x,y,z) indicating that this transition is dipole allowed perpendicular to the quasi-four fold rotation axis. Similar analysis shows that the 1s → $d(z^2)$ (A1) transition is dipole allowed parallel to the quasi-fourfold rotation axis, while the 1s → $d(x^2-y^2)$ transition is forbidden. We can thus have two dipolar contributions in the first pre-edge peak due to the 1s → π*(NO) and 1s → $d(z^2)$ as well as two quadrupolar contributions due to the 1s → $d(z^2)$ and 1s → $d(x^2-y^2)$ transitions. Since the latter are typically much weaker we will neglect them in our further discussion. In our experiment the X-ray polarization is perpendicular to the *c*-axis of the crystal and thus in the same plane as the quasi-fourfold rotation axis N–C–Fe–N–O (see Figure 1 of Ref. [25]). Since the four $[Fe(CN)_5NO]^{2-}$ molecules in the unit cell are oriented in pairs with an angle of approximately 70° between the N–C–Fe–N–O directions (within a pair the orientation of N–C–Fe–N–O is antiparallel within the *ab*-plane), both components parallel and perpendicular to the X-ray polarization are always present, independent of the rotation around the *c*-axis. Hence, we can consider the first pre-edge peak at 7114 eV as due to these dipolar allowed transition involving the LUMO and LUMO+1. The existence of pre-edge peaks due to back-bonding effects was recently elucidated by calculations of K-edge X-ray absorption spectra using the restricted active space method on $[Fe(CN)_6]^{n-}$ (n=3,4) [28]. Furthermore, Chergui and co-workers have investigated nitrosylmyoglobin

(MbNO) by XAS and TD-DFT calculations [29], where they found a single pre-edge feature, that is dominated by 1s → d(σ) and 1s → d(π) – π(NO)* transitions.

By irradiation with 476 nm, MS1 is populated, i.e. the NO ligand undergoes rotation from N-bound to O-bound to the Fe central atom. This rotation has a major effect on the back-bonding between Fe and NO, as now the NO is O-bound to Fe. The two major consequences are that the energy of the LUMO is lowered in MS1 (by approximately 0.6 eV) [9] and that the nature of the LUMO and LUMO+1 is slightly changed. Within our energy resolution we cannot observe an energetic shift of the pre-edge peak. The observed increase of the intensity of the pre-edge peak on the other hand is clearly visible and reproducible, and should therefore be reflected in the nature of the corresponding transition, i.e. the dipolar character should be increased. DFT calculations on the nature of the GS and MS1 state including analysis of the nature of the valence orbitals have been performed quite early by Buchs *et al.* [14c] and Atanasov *et al.* [14d]. Both indicate an increase of the contribution of Np and Op orbitals to the LUMO by almost 10% when going from GS to MS1, whereas the Fe d(xz,yz) contribution diminishes accordingly. Concerning the LUMO+1, there is less information available about expected changes in the nature of this MO. In the pDOS calculated in [9] there seems to be merely interchange of the Np and Op contributions, without significant change in the amount of this ligand contribution. Concerning the MS2, obtained via 1064 nm irradiation of MS1, the symmetry is reduced to $C_s$ and hence the LUMO is split into two orbitals with a' and a'' symmetry. Since the NO ligand is now rotated the nature of the MOs changes significantly in their composition. However, if one considers the total Np and Op contributions as calculated by Buchs *et al.* [14c] one obtains a value close to the GS (138% for GS, 139% for MS2; see Tables II, V and VI in [14c]) significantly lower than the MS1 value (150%). Hence, calculations predict an increase of about 10% in ligand p-contribution when going from GS to MS1.

Overall, the observed increase in the pre-edge peak intensity upon generation of MS1 and the subsequent decrease upon transfer to MS2 can thus be interpreted by the modified transition probability due to the change in nature of the LUMO. A more thorough analysis involving also the two other, higher-lying, pre-edge peaks will require additional measurements varying the orientation of the crystal with respect to the polarization of the X-ray beam, especially also along the crystallographic *c*-axis. This would also allow to detect potential quadrupolar contributions and to distinguish between dipole and quadrupole transitions [30].

The changes in the intensity of the pre-peak features can be used as an indicator for the successful generation of the MS1 and MS2 linkage isomers in SNP. Considering only one major contribution of dipolar nature due to the 1s → π*(NO) transition, the change in the pre-edge peak area can serve to deduce quantitative information about the amount of p-character of the LUMO. We observe an increase of 17% in peak area. Assuming a population of MS1 of 50% (maximum achievable for this state [7]) we would thus expect that the p-character of the LUMO increases by 34% when going from GS to MS1. This is much higher than the predicted change from theory (10%), but given the assumptions we made, this estimate is only a first rough approximation and in terms of absolute numbers the earlier calculations provide limited reliability also. So definitely, more measurements and corresponding dedicated calculations are

necessary for an in-depth quantitative evaluation. However, these results clearly show that information about the orbital character of frontier orbitals of photoinduced linkage isomers can be obtained from such XAS measurements under light illumination.

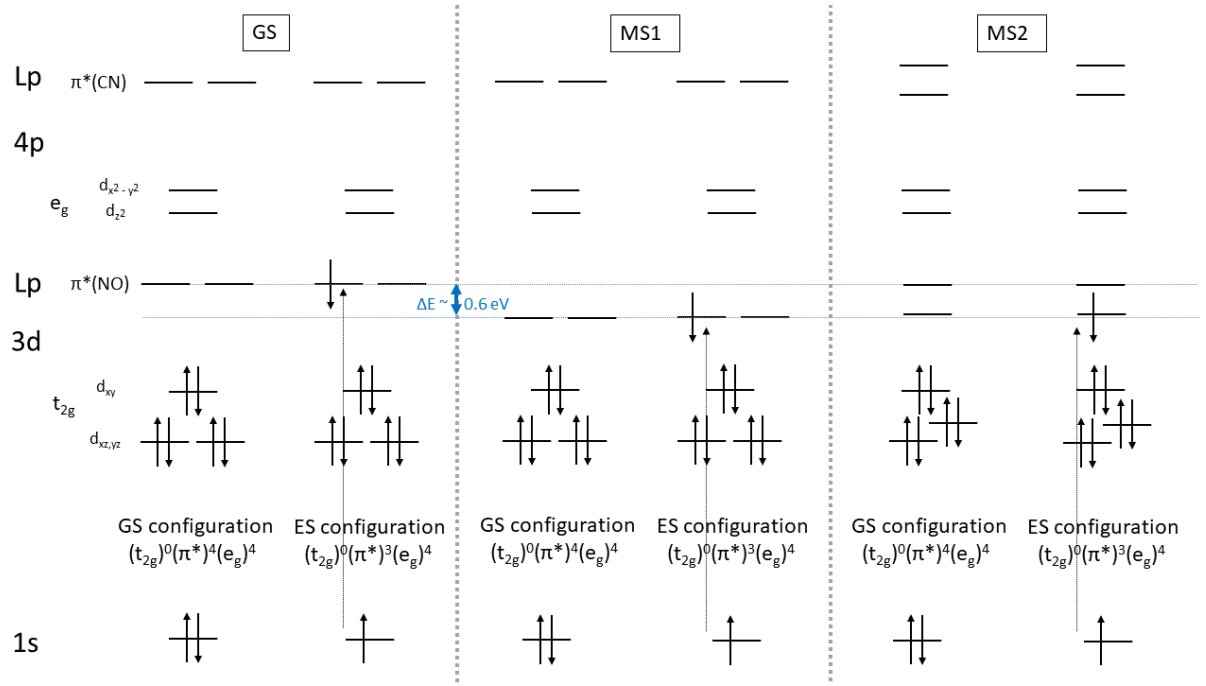


Figure 3. Scheme for the analysis of XANES measurements of SNP, using $C_{4v}$ symmetry for GS and MS1 and $C_s$ for MS2, for the three isomer configurations. Level ordering of iron (1s, 3d, 4p) and ligand (Lp) orbitals, with details of 3d and π*(NO) orbitals according to [9]. (Spacing between orbitals is **not** proportional to energy difference).

## Conclusions

Using a dedicated low-temperature setup allowing for in-situ irradiation of single crystals, it was demonstrated for the first time that polarized XAS is adequate for giving insight into the light-induced nitrosyl linkage isomers MS1 and MS2, as exemplarily shown on SNP. The analysis of the light-induced changes of the pre-edge peak intensity can be interpreted by the change in the nature of the frontier molecular orbitals due to the structural rearrangement, namely an increase in NO p-orbital contributions for MS1, which was expected from theoretical calculations and which increases the dipolar character and thus the transition probability. These observed intensity changes can serve as fingerprint and measure of successful linkage isomer generation in a XAS experiment, which is important since the population of the MS1 and MS2 depends on irradiation wavelength and other factors such as light polarization, penetration depth of light in the crystal, and temperature. Note however, that due to the rather small intensity changes, a quantitative exploitation and interpretation would rely ideally on a second indicator, that is measured in-situ. As a perspective, if one measures independently the population of the generated linkage isomers, e.g. by optical transmission, the observed change in peak area can be used to determine experimentally the change in the p-contribution to the first unoccupied molecular orbitals.

**Experimental Section**

Large single crystals of SNP were recrystallized by slow evaporation from aqueous solutions. Thin oriented plates were prepared by cutting plates of thickness 1 mm or less from the large crystals, perpendicular to the crystal axes identified from the naturally grown faces. These plates were then ground to thicknesses between 100 – 200 micrometers and finally polished to optical quality (see Figure 4a). The plates were oriented using polarized microscopy and their thickness was determined by micrometer screws. The crystals were then mounted on copper plates using Kapton tape in order to ensure good thermal contact. The copper plates are then mounted on a standard sample holder which can be screwed on the cold finger of the $LN_2$ cryostat (see Figure 4a). The cold finger of the cryostat can be rotated around the vertical axis (see Figure 4b) allowing to orient the face of the crystal with an appropriate angle towards the X-ray beam and at the same time towards the LASER source. Typical angles used in our experiment are between 30 – 50 degrees with respect to the incident X-ray beam. The XAS experiment requires an evacuated beam path. However, since SNP contains crystal water, exposure to vacuum at room temperature leads to the destruction of the crystals. In order to avoid this, the mounted crystals are cooled in a $N_2$ atmosphere to -40°C before the sample chamber is evacuated to $10^{-6}$ mbar. Then the sample is cooled slowly down to the measurement temperature of 77 K by adding liquid nitrogen to the reservoir in contact with the cold finger. The cold finger is then kept at 77 K by contact with the reservoir of liquid nitrogen during the whole measurement.

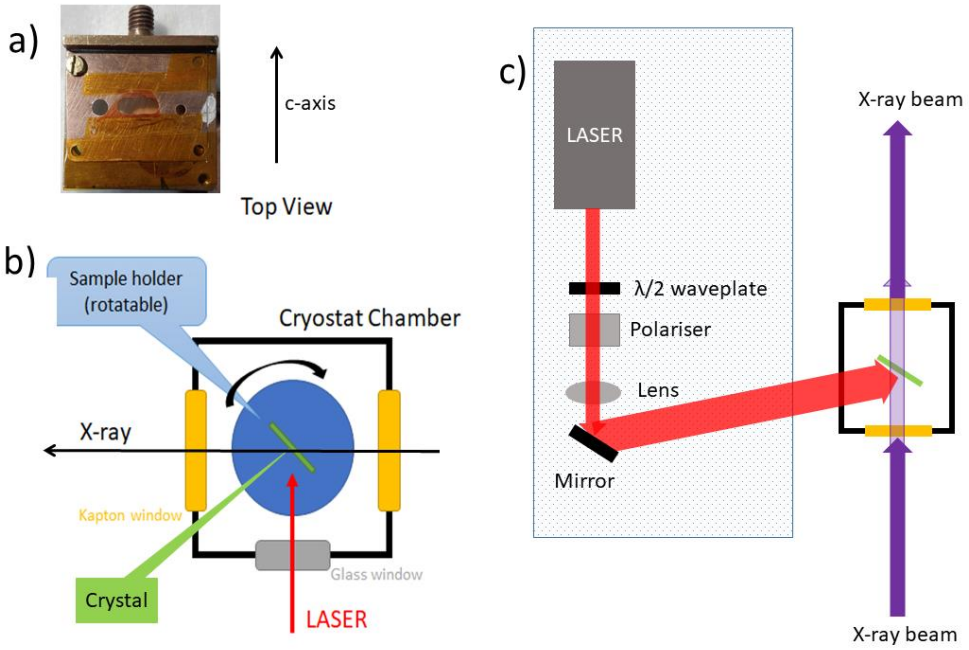


Figure 4: a) Photo of crystal (a-cut) mounted on the sample holder (copper plate) by Kapton tape in order to ensure good thermal contact; b) Schematics of the cryostat chamber in which the crystal is mounted on a cold finger; c) Schematics of the LASER setup with respect to cryostat and X-ray beam. The intensity and polarization direction of the LASER light is controlled via a λ/2 waveplate and a polarizer. The beam is expanded by a lens (LINOS, f=40 or 80 mm) in order to cover the whole sample size.

Irradiation by light is possible through a glass window (transparent in the visible and near infrared range), as schematically shown in Figure 4b,c. The intensity and polarization of the light beam is controlled by a λ/2 waveplate and polarizer. The beam is expanded by a lens to cover the whole crystal size and ensure homogenous illumination. Typical used light intensities are 20 mW/cm$^2$ in the blue-green spectral range (476 nm and 514 nm LASER) and 50 mW/cm$^2$ in the infrared spectral range (1064 nm LASER), to avoid overheating of the crystal. Polarization of the light is chosen along the *c*-axis of the crystals, to achieve maximum population of the PLI [7]. Using this polarization one can estimate the necessary exposure $Q = I \cdot t$ (units of J/cm$^2$) in order to reach saturation or at least a significant population of the metastable states MS1 and MS2 according to the results of Ref. [7]. For an intensity $I$ = 20 mW/cm$^2$ used for the irradiation with 476 nm, one obtains in one hour an exposure $Q$(1 hour) = 72 J/cm$^2$, while for the irradiation with 1064 nm at 50 mW/cm$^2$ the exposure after one hour is $Q$(1 hour) = 180 J/cm$^2$. As shown in [7] approximately 2000 J/cm$^2$ are needed to obtain 40% MS1 with 476 nm for a 330 μm crystal. Since we use thinner crystals population will be faster (due to better penetration of light throughout the whole crystal), and therefore an exposure of approximately 1000-1500 J/cm$^2$ is sufficient [9]. After 15 hours of irradiation at this intensity one reaches 1080 J/cm$^2$. For the transfer from MS1 to MS2 with 1064 nm less exposure is needed [7,11b], after about 120 - 250 J/cm$^2$ a maximum of MS2 is obtained, followed by a very slow depopulation of MS2 back to GS. Using 50 mW/cm$^2$ at 1064 nm, 90 minutes of irradiation, yielding 270 J/cm$^2$, are thus sufficient to transfer MS1 to MS2. The X-ray beam enters the cryostat chamber through a Kapton window (see Figure 4b,c).

XAS measurements were performed in transmission mode at a low temperature 77 K, at the Fe K edge (7112 eV) at the XAFS beamline at the synchrotron ELETTRA (Trieste, Italy). Details of the XAFS beamline layout can be found in Ref. [31]. XAS data were acquired with the storage ring operating at 2.4 GeV yielding a current of 158.5 mA. A double crystal silicon Si (111) monochromator was used with a detuning of 0.3 for harmonic rejection. Iron metal foil was used to calibrate the monochromator. The energy resolution $\Delta$E/E was about $10^{-4}$. The first inflexion point of the XANES spectrum was assigned to 7112 eV corresponding to the edge energy of iron. A mixture of Ar, $N_2$ and He was used at the energy of 7000 eV to fill the ions chambers such that an absorption of 10%, 80% and 95% is obtained in the $I_0$, $I_1$, and $I_2$ chambers, respectively. The LASER irradiation time ranged between 0 to 15 hours for all samples and four scans were collected for XAS data.

The preliminary treatment of the XAS absorption spectra was performed in Athena software [32]. In order to improve statistics the four scans were averaged. The normalization process consisted of subtracting the pre-edge, post-edge and background signals from the experimental X-ray absorption spectrum.

The peak fitting method was used for fitting the peaks in the pre-edge region. Since the main objective of the analysis was to determine the change in the area of the pre-edge peak as a function of light exposure, the fit was performed with a single Gaussian function for the first pre-edge peak at 7114 eV, and a baseline, by keeping the number of variables as low as reasonably possible (see Figure 5 for an example of this fit on the GS). The series of pre-edge

peaks as a function of exposure *Q* was treated in the same manner keeping strictly the same number of variables and the same type of background and peak shape (Gaussian). The spectra were vertically shifted to have the same value at 7108.09 eV (chosen to be zero). The fit has been performed between 7108.09 and 7118.08 eV.

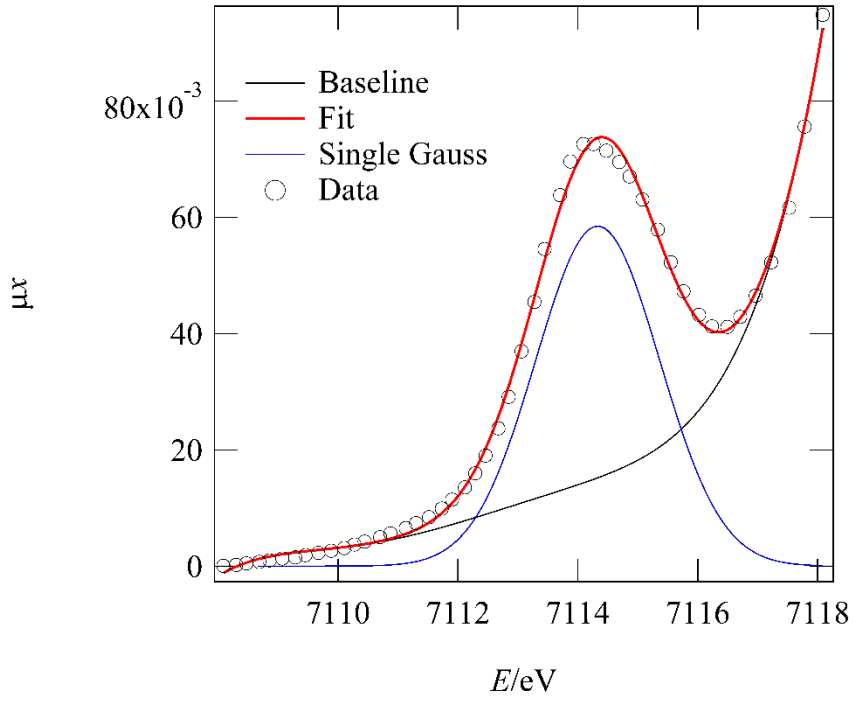


Figure 5: Example of pre-edge peak fit with single Gaussian, GS at 77 K.

**Acknowledgments**
The experiments at the synchrotron ELETTRA (Trieste, Italy) have been supported through the granted proposal 20195169 and sponsored by ICTP-ELETTRA users support.
Duclair Tchana Kamgne and Bridinette Thiodjio Sendja are grateful to IUPAP-IUCr-LAAAMP within the ICSU Grants Programme 2016-2019 in a *Continuing User Award project*, who provided them the support for their training at the ELETTRA Synchrotron.
The authors are also grateful to the XAFS beamline staff (Dr Simone Pollastri, Mr Luca Olivi and Mr Ricardo Grisonich) of Elettra Sincrotrone (Trieste, Italy) for on-site support.

**Keywords**. Photoinduced linkage isomers, X-ray absorption spectroscopy, nitrosyl, iron, sodium nitroprusside.

## References


[1] a) L. M. Loftus, K. F. Al-Afyouni, C. Turro, *Chem. Eur. J.* **2018**, *24*, 11550-51553; b) K. Sato, K. Ando, S. Okuyama, S. Moriguchi, T. Ogura, S. Totoki, H. Hanaoka, T. Nagaya, R. Kokawa, H. Takakura, M. Nishimura, Y. Hasegawa, P. L. Choyke, M. Ogawa, and H. Kobayashi, *ACS Central Science* **2018**, *4*, 1559-1569.

[2] a) P. A. Thomas, K. S. Menghrajani, W. L. Barnes, *Nat. Commun.* **2022**, *13*, 1809-51553; b) S. Garg, H. Schwartz, M. Kozlowska, A. B. Kanj, K. Müller, W. Wenzel, U. Ruschewitz, L. Heinke, *Angew. Chem. Int. Ed.* **2019**, *58*, 1193-1197; c) H. Dong, H. Zhu, Q. Meng, X. Gong, W. Hu, *Chem. Soc. Rev.* **2012**, *41*, 1754-1808.

[3] a) M. J. Rose, P. J. Mascharak, *Curr. Opin. Chem. Biol.* **2008**, *12*, 238-244; b) I. Stepanenko, M. Zalibera, D. Schaniel, J. Telser, V. B. Arion, *Dalton Trans.* **2022**, *51*, 5367-5393; c) D. Schaniel, M. Imlau, T. Weisemoeller, T. Woike, K. W. Krämer, H. U. Güdel, *Adv. Mater.* **2007**, *19*, 723-727.

[4] A. Hasil, D. Beck, D. Schröder, S. Pillet, E. Wenger, T. Woike, P. Klüfers, D. Schaniel, *Angew. Chem. Int. Ed.* **2022**, published online DOI: https://doi.org/10.1002/anie.202210671

[5] J. H. Enemark, R. D. Feltham, *Coord. Chem. Rev.* **1974**, *13*, 339-406.

[6] P. Coppens, I. Novozhilva, A. Kovalevsky, *Chem. Rev.* **2002**, *102*, 861-883.

[7] T. Woike, W. Krasser, H. Zöllner, W. Kirchner, S. Haussühl, *Z. Phys. D* **1993**, 25, 351-356.

[8] a) D. Schaniel, T. Woike, B. Delley, C. Boskovic and H.-U. Güdel, *Phys. Chem. Chem. Phys.* **2005**, *7*, 1164-1170; b) H. Zöllner, W. Krasser, T. Woike, S. Haussühl, Chem. Phys. Lett. **1989**, *161*, 497; c) B. Cormary, S. Ladeira, K. Jacob, P. G. Lacroix, T. Woike, D. Schaniel and I. Malfant*, Inorg. Chem.* **2012**, *51*, 7492–7501; d) A. A. Mikhailov, G. A. Kostin, D. Schaniel, *New J. Chem.* **2022**, 46, 12641-12650.

[9] D. Schaniel, J. Schefer, B. Delley, M. Imlau and T. Woike, *Phys. Rev. B* **2002**, *66*, 085103.

[10] T. Woike, W. Krasser, P. S. Bechthold, S. Haussühl, *Phys. Rev. Lett.* **1984**, *53*, 1767-1770.

[11] a) H. Zöllner, T. Woike, W. Krasser, S. Haussühl, *Z. Kristallogr.* **1989**, *188*, 139-153; b) D. Schaniel, T. Woike, L. Tsankov, M. Imlau, *Thermochim. Acta* **2005**, *429*, 19-23.

[12] a) Th. Woike, W. Kirchner, H. Kim, S. Haussühl, V. Rusanov, V. Angelov, S. Ormandjiev, Ts. Bonchev, A. N. F. Schroeder*, Hyp. Inter.* **1993**, *77*, 265-275; b) Th. Woike, M. Imlau, V. Angelov, J. Schefer, B. Delley, *Phys. Rev. B* **2000**, *61*, 12249.

[13] a) M. D. Carducci, M. R. Pressprich, P. Coppens, *J. Am. Chem. Soc.* **1997**, *119*, 2669-2678; b) D. Schaniel, Th. Woike, J. Schefer, V. Petříček, *Phys. Rev. B* **2005**, *71*, 174112; c) D. Schaniel, Th. Woike, J. Schefer, V. Petříček, K. W. Krämer, H. U. Güdel*, Phys. Rev. B* **2006**, *73*, 174108.

[14] a) B. Delley, J. Schefer, Th. Woike, *J. Chem. Phys.* **1997**, *107*, 10067-10074; b) P. Blaha, K.-H. Schwarz, W. Faber, J. Luitz, *Hyp. Inter.* **2000**, *126*, 389-395; c) M. Buchs, C. A. Daul, P. T. Manoharan, C. W. Schläpfer, *Int. J. Quant. Chem.* **2002**, *91*, 418-431; d) M. Atanasov, T. Schönherr, *J. Mol. Struct.* **2002**, *592*, 79-93.

[15] a) D. Schaniel, Th. Woike, C. Merschjann, M. Imlau, *Phys. Rev. B* 2005, *72*, 175119; b) D. Schaniel, M. Nicoul, Th. Woike, *Phys. Chem. Chem. Phys.* **2010**, *12*, 9029-9033; c) G. Galle, M. Nicoul, Th.

Woike, D. Schaniel, E. Freysz, *Chem. Phys. Lett.* **2012**, *552*, 64-68; d) M. S. Lynch, M. Cheng, B. E. Van Kuiken, M. Khalil, *J. Am. Chem. Soc.* **2011**, *133*, 5255-5262; e) A. A. Raheem, M. Wilke, M. Borgwardt, N. Engels, S. I. Bokarev, G. Grell, S. G. Aziz, O. Kühn, I. Y. Kiyan, C. Merschjann, E. F. Aziz, *Struct. Dyn.* **2017**, *4*, 044031.

[16] N. Casaretto, D. Schaniel, P. Alle, E. Wenger, P. Parois, B. Fournier, E.-E. Bendeif, C. Palin, S. Pillet, *Acta Cryst. B* **2017**, *73*, 696-707.

[17] M. L. Baker, M. W. Wara, J. J. Yan, K. O. Hodgson, B. Hedman, E. I. Solomon, *Coord. Chem. Rev.* **2017**, *345*, 182-208.

[18] a) G. Poneti, M. Mannini, L. Sorace, P. Sainctavit, M.-A. Arrio, A. Rogalev, F. Wilhelm, A. Dei, *ChemPhysChem* **2009**, *10*, 2090-2095; b) D. M. Pajerowski, B. Ravel, C. H. Li, M. F. Dumont, D. R. Talham, *Chem. Mater.* **2014**, *26*, 2586–2594.

[19] a) T. Yokoyama, M. Kiguchi, T. Ohta, O. Sato, Y. Einaga, K. Hashimoto, *Phys. Rev. B* **1999**, *60*, 9340; b) X.-D. Ma, T. Yokoyama, T. Hozumi, K. Hashimoto, S. Okhoshi, *Phys. Rev. B* **2005**, *72*, 094107.

[20] T. Yokoyama, H. Tokoro, S. Okhoshi, K. Hashimoto, K. Okamoto, T. Ohta, *Phys. Rev. B* **2002**, *66*, 184111.

[21] S. Della Longa, A. Arcovito, B. Vallone, A. C. Castellano, R. Kahn, J. Vicat, Y. Soldo, J. L. Hazemann, *J. Synchrotron Rad.* **1999**, *6*, 1138-1147.

[22] a ) C.Bressler, M. Chergui, *Ann. Rev. Phys. Chem.* **2010**, *61*, 263-282; b) E. Borfecchia, C. Garino, L. Salassa, C. Lamberti, *Phil. Trans. R. Soc. A* **2013**, *371*, 20120132.

[23] W. Gadeke, E.E. Koch, G. Drager, R. Frahm, V. Saile, *Chem. Phys.* **1988**, *124*, 113-119.

[24] S. Nanba, D. Asakura, M. Okubo, H. Zhou, K. Amemiya, K. Okada, P.-A. Glans, C. A. Jenkins, E. Arenholz, J. Guo, *Phys. Chem. Chem. Phys.* **2014**, *16*, 7031–7036.

[25] D. Tchana Kamgne, B. Thiodjio Sendja, D. Olivera de Souza, D. Schaniel, G. Aquilanti, *J. Mol. Struct.* **2021**, *1245*, 131119.

[26] T. Yamamoto, *X-ray Spectrom.* **2008**, *37*, 572-584.

[27] P. T. Manoharan, Harry B. Gray, *J. Am. Chem. Soc.* **1965**, *87*, 3340–3348.

[28] M. Guo, L. K. Sørensen, M. D. Delcey, R. V. Pinjari, M. Lundberg, *Phys. Chem. Chem. Phys.* **2016**, *18*, 3250-3259.

[29] F. A. Lima, T. J. Penfold, R. M. van der Veen, M. Reinhard, R. Abela, I. Tavernelli, U. Rothlisberger, M. Benfatto, C. J. Milne, M. Chergui, *Phys. Chem. Chem. Phys.* **2014**, *16*, 1617-1631.

[30] a) T. E. Westre, P. Kennepohl, J. G. DeWitt, B. Hedman, K.O. Hodgson, E. I. Solomon, *J. Am. Chem. Soc.* **1997**, *119*, 6297-6314; b) C. Brouder, *Phys. Condens. Matter* **1990**, *2*, 701-738.

[31] A. Di. Cicco, G. Aquilanti, M. Minicucci, E. Principi, N. Novello, A Cognigni, L. Olivi, *J. Phys. Conf. Ser.* **2009**, 190, 012043.

[32] B. Ravel and M. Newville, *J. Synchrotr. Rad.* **2005**, *12*, 537–541.